JOURNAL OF MATERIALS SCIENCE 33 (1998) 4213–4224

Micromechanics of multiple cracking

Part I *Fibre analysis*

J. KULLAA
VTT Building Technology, P.O. Box 18071, FIN-02044 VTT, Finland
E-mail: jyrki.kullaa@vtt.fi

Fibre-reinforced brittle materials exhibiting a strain-hardening tensile behaviour undergo a multiple cracking process. A micromechanical analysis of a straight smooth fibre, bridging one or several cracks in a multiply-cracked composite is introduced, taking into account the full or elastic bond, gradual debonding, and frictional sliding of the fibre. Equilibrium is satisfied by means of a two-fibre system introducing a symmetry fibre within the segment. Equations for different debonding cases are derived. The fibre ends are analysed using a simplified approach, the validity of which is discussed. The system equations are derived from the compatibility condition of equal crack widths. Two examples are analysed to study the effects of crack spacing.

Nomenclature

A_f	= area of fibre
A_m	= area of matrix
d	= fibre diameter
E_f	= modulus of elasticity of fibre
E_m	= modulus of elasticity of matrix
F, F_1, F_2	= tensile force distributions in fibres
K	= $\psi\kappa/2A_mE_m$
l	= fibre embedded length or segment length
l_f	= fibre length
l_1, l_2	= fibre debonded lengths
P, P_1, P_2	= fibre forces at the cracks
$\hat{Q}$	= $1 + 2A_mE_m/A_fE_f$
S	= slip between fibre and matrix
s	= half of segment length
T	= tensile forces in matrix
t_f	= frictional shear flow
u	= rigid body displacement of fibre
V_f	= fibre volume fraction
w	= crack width
x	= coordinate along segment
Δ	= relative displacement of fibre at crack
ε_f	= strain in fibre
ε_m	= strain in matrix
κ	= bond modulus
$\hat{\lambda}$	= $(\hat{K}\hat{Q})^{1/2}$
λ_1	= $[\hat{K}(\hat{Q}-1)]^{1/2}$
λ_2	= $[\hat{K}(\hat{Q}+1)]^{1/2}$
ψ	= perimeter of the fibre
σ_{nim}	= tensile strength of the matrix
τ	= shear stress between fibre and matrix
τ_f	= frictional shear stress between fibre and matrix
τ_u	= shear strength between fibre and matrix

1. Introduction

Composites have become important materials in the construction industry, as well as in other fields like the automotive, space and engineering industries. Brittle materials, such as concrete and ceramics reinforced with fibres, exhibit ductile behaviour after cracking and are therefore gaining increasing interest among engineers. Before designing structures for new applications meeting certain requirements, the behaviour of the material must be known.

Fibres are effective primarily after cracking, where they bridge the crack. With randomly oriented short fibres added to the mix, the composite usually fails in a single fracture mode, improving the ductility of the material. However, the improvements in strength or strain capacity are insignificant. To increase them, the fibres at the crack must be able to sustain the load needed for crack formation without being broken or pulled out of the matrix. If this condition is fulfilled, the matrix fails successively and divides into segments of similar lengths. This process is called multiple cracking. Beyond the multiple cracking stage, the composite shows strain-hardening behaviour until crack localization occurs due to fibre breakage or pull-out.

The multiple cracking process and subsequent strain-hardening behaviour can be produced by tailoring some of the material parameters. First, the usage of continuous and aligned fibres [1] leads perhaps to the highest strength. The main disadvantage is the difficulty and cost of processing. Second, the fibre content of randomly oriented, discontinuous fibres can be increased until the mix becomes too stiff to produce [2, 3]. Third, fibres with a high aspect ratio, l_f/d, can be used, where l_f and d are the fibre length and the fibre diameter, respectively [4]. However, the

higher the aspect ratio, the lower the fibre volume content that can be incorporated into the mix [5]. Fourth, improving the bond properties to prevent fibre pull-out can lead to a multiple cracking process, unless the fibres break as the crack forms. The bond can be increased either chemically by affecting the bond characteristics, or mechanically using deformed fibres [6].

There are quite a number of computational models for the fibre pull-out problem [7–14]. They can be used to model the constitutive behaviour, or the stress–crack width relation of composites failing by a single fracture mode [7, 13, 15–17]. However, in the modelling of multiply-cracked composites, if the fibre extends over several cracks, the boundary conditions differ from those of the above fibre pull-out problem. Analytical models for multiple cracking have been presented by Aveston *et al.* [1] for composites with continuous aligned fibres, assuming a frictional bond; Aveston and Kelly [18] for composites with non-parallel, continuous fibres taking into account the elastic bond and partial debonding; Aveston *et al.* [5] and Kullaa [17] for short random fibres assuming a frictional bond; Tjiptobroto and Hansen [3, 19] who defined the energy terms during cracking for composites with random discontinuous fibres; Li and Leung [20] who stated the conditions for steady-state cracking; and Li *et al.* [21] who utilized the energy approach of fracture mechanics to study matrix cracking and debonded length of continuous aligned fibres.

To analyse the mechanical behaviour of fibre-reinforced brittle materials, a new micromechanical model of the multiple cracking process is introduced. It is based on the analysis of a single fibre with a random location and orientation bridging one or several cracks. Because the forces in the fibre at the adjacent cracks may differ, the existence of a symmetry fibre is assumed to satisfy equilibrium conditions. The symmetry fibre was first introduced by Kullaa [17] for a purely frictional bond, and [22] for elastic or full bond. In the present study, the gradual debonding and sliding of the fibre is introduced and analysed. Different cases must be analysed, depending on the lengths of the debonded zones. Debonding is assumed to initiate if the interface shear stress exceeds the interfacial shear strength as proposed by Naaman *et al.* [8], Lim *et al.* [13], and Leung and Li [10]. Stang *et al.* [11] and Leung [9] also proposed a fracture-based debonding theory, and compared the two theories. They found that both analyses are identical, provided the effective shear strength is chosen. After debonding a constant frictional shear stress is assumed (Figure 1).

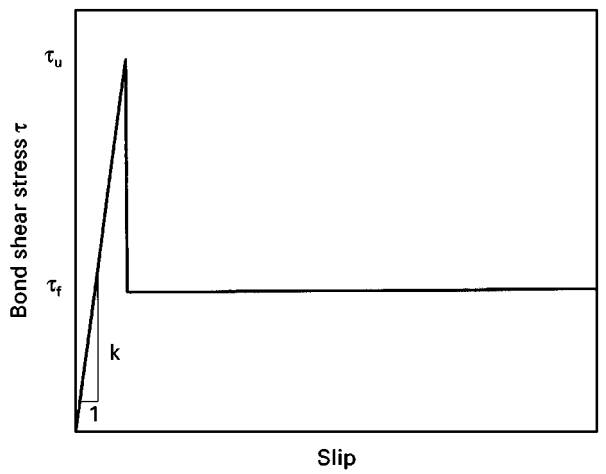

Figure 1 Assumed bond-slip relation between fibre and matrix.

In the elastic or full bond stage, a linear relationship between the interface shear stress and the relative displacement between the fibre and the matrix is chosen [8, 11–13, 18, 22–25]. This constitutive relation leads to a linear relationship between the pull-out load and the fibre end displacement. However, the coefficient, or the bond modulus, is not a constant but depends on the fibre diameter, the fibre volume content, and the moduli of elasticity of the fibre and the matrix [26].

In a multiply-cracked composite, the crack widths and crack spacings are assumed to be equal. The assumption of equal crack widths is justified for a composite exhibiting strain-hardening behaviour, because the distribution of fibres is supposed to be equal at every crack. However, in the strain-softening stage, crack localization occurs, causing one crack to open whereas the others close. The widths of the closing cracks can be assumed to be mutually equal. If the crack width is fixed, the fibre forces at the cracks can be solved and the distributions of the forces in the fibre and the matrix as well as the interfacial shear stress computed.

2. A two-fibre system

Leung [9] stated that if the stress gradient between adjacent fibres is small, the shear stress in the matrix halfway between the fibres can be taken as zero. The

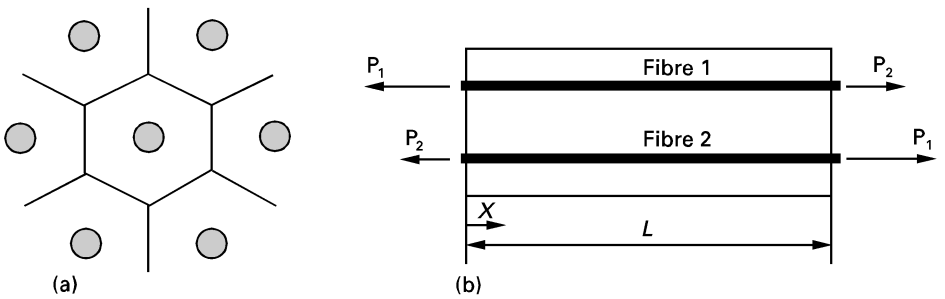

Figure 2 Hexagonal fibre arrangement and the fictitious two-fibre system.

fibres can then be treated as independent. This assumption is only justified if the fibres are pulled out in the same direction, which is the case in a single fracture mode.

In multiply-cracked discontinuous fibre composites with a fibre bridging two adjacent cracks, the fibre forces at the cracks may differ and thus be out of balance. It follows that the shear stress in the matrix halfway between the fibres must be different from zero, because of a stress transfer from the fibre to other fibres in order to satisfy the equilibrium condition. This also means that fibres cannot be analysed independently, but the interaction must be taken into account. Let A_f and A_m be the cross-sectional areas of a fibre and its surrounding matrix, respectively. Supposing that every fibre interacts with n surrounding fibres, for example $n = 6$ for a hexagonal fibre array shown in Fig. 2a, a single fibre interacts, on average, with a total fibre area of A_f via a matrix area of $2A_m$. The surrounding fibres can then be modelled as a single fibre with a total cross-sectional area of A_f together with its surrounding matrix area of A_m. The arrangement of fibres need not be hexagonal, nor the fibres aligned, because only an average stress in the matrix is considered. Only a constant fibre volume content in every cross-section of the composite is assumed.

This leads to the introduction of a fictitious two-fibre system, with two fibres being analysed simultaneously. For the equilibrium condition, the choice of one crack force in the second fibre is arbitrary, the other depending on this choice. Because the second fibre represents surrounding fibres, an average fibre should be chosen. However, the average force distribution in a fibre is unknown. Therefore, the second fibre is idealized as having a symmetrical force distribution which is a mirror image of that in fibre 1 (Fig. 2b) [22]. The problem with two symmetrical fibres is relatively simple to analyse, and satisfies the force equilibrium. However, the assumption of a symmetry fibre may lead to inaccuracy in relative fibre displacements, if the fibre force is much different from the average. In the average sense, the error probably decreases when deriving the macromechanical behaviour considering all fibres.

The analysis of a two-fibre system is as follows. In the case of an elastic bond between fibre 1 and the matrix, a second-order differential equation for the fibre force F_1 is derived [22]

$$\frac{d^2F_1(x)}{dx^2} = -\hat{K}P + \hat{K}\hat{Q}F_1(x) + \hat{K}F_2(x) \tag{1}$$

with

$$\hat{K} = \frac{\psi\kappa}{2A_mE_m} \tag{2}$$

$$\hat{Q} = 1 + \frac{2A_mE_m}{A_fE_f} \tag{3}$$

where F_1 and F_2 are the tensile forces in fibres 1 and 2, respectively; $P = P_1 + P_2$ is the sum of the fibre forces at the crack, or the total load ($P_1 = F_1(0) = F_2(l)$, and $P_2 = F_1(l) = F_2(0)$, where l is the segment length or crack spacing); E_f and E_m are the moduli of elasticity of the fibre and the matrix, respectively; ψ is the perimeter of the fibre, and κ the bond modulus, defined by

$$\tau = \kappa S \tag{4}$$

where τ is the interfacial shear stress between the fibre and the matrix and S is the relative displacement between the fibre and the matrix.

2.1. Elastic bond in both fibres

If the bond also between fibre 2 and the matrix is elastic, a differential equation similar to equation 1 can be derived for fibre force F_2. The distributions of the fibre forces can then be solved from fourth-order differential equations [22], and read

$$F_1(x) = Ae^{-\lambda_1 x} + Be^{\lambda_1 x} + Ce^{-\lambda_2 x} + De^{\lambda_2 x} + \frac{P}{\hat{Q}+1} \tag{5}$$

$$F_2(x) = -Ae^{-\lambda_1 x} - Be^{\lambda_1 x} + Ce^{-\lambda_2 x} + De^{\lambda_2 x} + \frac{P}{\hat{Q}+1} \tag{6}$$

where

$$\lambda_1 = [\hat{K}(\hat{Q}-1)]^{1/2} \tag{7}$$

$$\lambda_2 = [\hat{K}(\hat{Q}+1)]^{1/2} \tag{8}$$

The coefficients A, B, C, and D are determined from the boundary conditions.

2.2. Frictional bond in the other fibre

If the bond between fibre 1 and the matrix is elastic and only constant frictional between fibre 2 and the matrix, the analysis is as follows. The differential Equation 1 for F_1 still holds and becomes

$$\frac{d^2F_1(x)}{dx^2} - \hat{K}\hat{Q}F_1(x) = \hat{K}[F_2(x) - P] \tag{9}$$

Because $F_2(x)$ is a polynomial of first order, the solution of the differential equation 9 takes the form

$$F_1(x) = Ge^{\hat{\lambda}x} + He^{-\hat{\lambda}x} + \frac{1}{\hat{Q}}[P - F_2(x)] \tag{10}$$

where

$$\hat{\lambda} = [\hat{K}\hat{Q}]^{1/2} \tag{11}$$

and the coefficients G and H are determined from the boundary conditions. Corresponding equations can be derived for the case of a full bond between fibre 2 and the matrix and frictional bond between fibre 1 and the matrix.

3. System equations

The relative displacement of the fibre at the crack can be expressed by a sum of three terms: the relative displacement of the fibre at an arbitrary position within the segment, the increase of the displacement from that point to the crack, and the elastic elongation of the fibre at the crack. Mathematically, this can be

written for the left and right sides of the crack, respectively, as

$$\Delta_i^{\mathrm{l}} = S_i|_{x=l-l_2^i} + \int_{l-l_2^i}^{l} (\varepsilon_{\mathrm{f}} - \varepsilon_{\mathrm{m}})\,\mathrm{d}x + \frac{P_i}{A_{\mathrm{f}}E_{\mathrm{f}}}\,u_i \tag{12}$$

$$\Delta_i^{\mathrm{r}} = S_{i+1}|_{x=l_1^{i+1}} + \int_{l_1^{i+1}}^{0} (\varepsilon_{\mathrm{f}} - \varepsilon_{\mathrm{m}})\,\mathrm{d}x + \frac{P_i}{A_{\mathrm{f}}E_{\mathrm{f}}}\,u_{i+1} \tag{13}$$

where Δ_i^{l} and Δ_i^{r} are the relative displacements of the fibre at the left and right side of crack i, respectively, ε_{f} and ε_{m} are the strains in the fibre and the matrix, respectively, l_1^{i+1} is the debonded length at the left end of segment $i+1$ and l_2^i is the debonded length at the right end of segment i.

The last terms in Equations 12 and 13 are the elastic elongations of the fibre at the crack, u_i being the rigid body displacement of the fibre within segment i, and P_i the force in the fibre at crack i. It should be noted that u_i is only non-zero if the fibre slides within the segment. Numbering of the cracks and segments is such that the crack i is located immediately to the right of segment i (see Fig. 3). The first terms in Equations 12 and 13 are the relative displacements at point $x = l - l_2^i$ in segment i and at point $x = l_1^{i+1}$ in segment $i+1$, respectively.

Before complete debonding and fibre sliding, the displacements at the ends of the full bond region are

$$S_i|_{x=l-l_2^i} = \frac{1}{\psi\kappa}\frac{\mathrm{d}F}{\mathrm{d}x}\bigg|_{x=l-l_2^i}. \tag{14}$$

$$S_{i+1}|_{x=l_1^{i+1}} = \frac{1}{\psi\kappa}\frac{\mathrm{d}F}{\mathrm{d}x}\bigg|_{x=l_1^{i+1}}. \tag{15}$$

After complete debonding from one side of the crack only, the fibre slides within the segment, and the first terms in Equations 12 and 13 become, respectively

$$S_i|_{x=l-l_2^i} = u_i \tag{16}$$

$$S_{i+1}|_{x=l_1^{i+1}} = u_{i+1} \tag{17}$$

It should be noted that if the fibre slips to the left within the segments i and $i+1$, the debonded lengths are $l_1^{i+1} = l$ and $l_2^i = 0$. The second term in Equation 12 is then zero, and the integration over the whole segment is carried out only to compute the displacement Δ_i^{r} at the right side of the crack. Similarly, if the fibre slips to the right, $l_1^{i+1} = 0$ and $l_2^i = l$, the second term in Equation 13 becomes zero, and the integration is only needed to compute Δ_i^{l}

The unknown variables are the rigid body motions u_i, and the fibre forces at the cracks. To solve the unknowns, the compatibility conditions between them are needed. They are obtained from the relative displacements by setting the crack widths equal to w

$$\Delta_i^{\mathrm{l}} - \Delta_i^{\mathrm{r}} = w \tag{18}$$

The last terms in Equations 12 and 13 consist of a product of the unknown variables. Therefore, Equation 18 becomes non-linear. The other terms in Equations 12 and 13 are linear with P_i, as shown in the Appendix. Fortunately, the non-linear terms are usually much smaller than the terms 16 and 17, and can therefore be ignored.

If the fibre slides within the segment i, the unknown rigid body displacement u_i is not equal to zero. Therefore, an additional equation must be stated. It is derived by assigning a constraint equation between the forces in the fibres at the adjacent cracks

$$P_i = P_{i-1} + t_{\mathrm{f}} l \tag{19}$$

where t_{f} is the frictional shear flow ($t_{\mathrm{f}} = \tau_{\mathrm{f}}\psi$), having a sign which depends on the direction of friction. If the fibre ends slip, the embedded length decreases with the rigid body displacement u. Thus the additional equations for the left and right ends, respectively are:

$$P_1 = t_{\mathrm{f}}(l_1^* - u_1) \tag{20}$$

$$P_n = -t_{\mathrm{f}}(l_{n+1}^* + u_{n+1}) \tag{21}$$

where l_1^* and l_{n+1}^* are the fibre embedded lengths within the fibre end segments. The differences in the signs of u are due to the fact that u is positive to the right. If the ends of the fibre and its symmetry fibre overlap, there will be two regions to be analysed – the overlapping and the non-overlapping one. Between them, the compatibility condition is as in Equation 18, the right-hand side now being zero.

The compatibility condition 18, and Equations 19, 20 and 21 lead to a system of equations, one or two per crack, depending on whether or not the fibre slides within the segment. If the fibre does not slide within segment i, the rigid body displacement u_i is zero, and the corresponding equation is ignored. For illustrative reasons, it is assumed that at the right fibre end the embedded length extends beyond the middle of the segment so that the fibre and its symmetry fibre partially overlap, but that at the left side they do not overlap (see Fig. 3). For a fibre bridging $n-1$ cracks, the equation then becomes

$$\begin{bmatrix}
t_{\mathrm{f}} & 1 & & & & & & & & \\
1 & c_{11} & -1 & c_{12} & & & & & & \\
 & -1 & & 1 & & & & & & \\
 & c_{21} & 1 & c_{22} & -1 & c_{23} & & & & \\
 & & & -1 & & 1 & & & & \\
 & & & & & & \ddots & & & \\
 & & & & & & c_{n-1,n-2} & 1 & c_{n-1,n-1} & -1 & c_{n-1,n} \\
 & & & & & & & & -1 & & 1 \\
 & & & & & & & & c_{n,n-1} & 1 & c_{nn} & -1 \\
 & & & & & & & & & & -1 & -t_{\mathrm{f}}
\end{bmatrix}$$

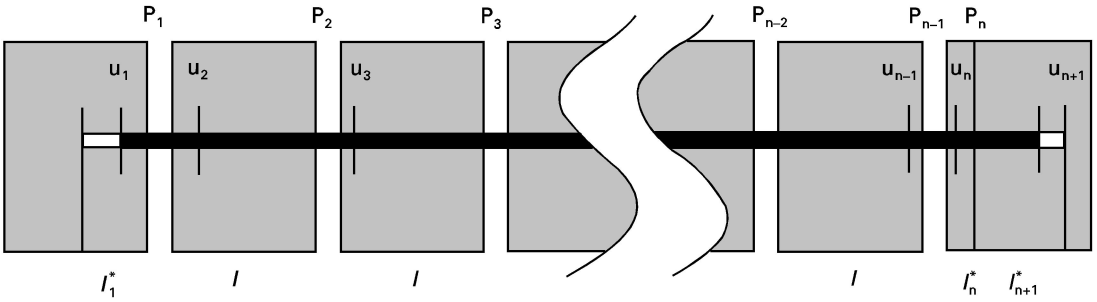

Figure 3 A model of crack bridging.

$$\begin{Bmatrix} u_1 \\ P_1 \\ u_2 \\ P_2 \\ u_3 \\ P_3 \\ \vdots \\ P_{n-2} \\ u_{n-1} \\ P_{n-1} \\ u_n \\ P_n \\ u_{n+1} \end{Bmatrix} = \begin{Bmatrix} t_f l_1^* \\ w \\ t_f l \\ w \\ t_f l \\ w \\ \vdots \\ w \\ t_f l \\ w \\ t_f l_n^* \\ 0 \\ t_f l_{n+1}^* \end{Bmatrix} - \{\boldsymbol{R}\} \qquad (22)$$

where l_n^* and l_{n+1}^* are the non-overlapping and the overlapping lengths of the right end, respectively. The terms c_{ij} are the coefficients of the fibre forces at the cracks, i referring to the displacement Δ_i at the crack i, and j referring to the force P_j at the crack j. The coefficients are sums of two terms, one for either side of the crack, and are obtained from the analysis of the relative displacements at the cracks. They are calculated for fixed debonded lengths which, in fact, are unknown and are solved by iteration from the shear stress conditions as outlined in the following section. The right-hand vector $\boldsymbol{R}$ consists of the constant terms of the functions for the displacements at the cracks. The derivation of the displacements for one case is shown in the Appendix.

4. Solution strategy

In addition to the variables in Equation 22, the lengths of the debonded zones are unknown as well. In this study, the strength-based theory is used, which means that the bond fails when the interfacial shear stress between the fibre and the matrix exceeds the bond strength. It should be noted that the same theory remains valid when using a fracture-based theory, i.e. the bond fails when the energy release rate at the interface exceeds a given threshold value [9, 11]. In that case the threshold value is not constant but depends also on the fibre diameter and the fibre volume content. Within the debonded zone, a frictional bond with a constant shear stress is assumed.

The condition for the debonded lengths is that once debonding has started, the shear stress at the end of the elastic region must be equal to the bond strength. The equation thus formed is non-linear and is solved iteratively by increasing the debonded lengths gradually.

Other conditions for the debonded lengths are as follows: if the shear stress at the end of the elastic zone is less than the frictional stress, the bond is assumed to return to elastic at that point. This "re-bonding" process is gradually continued, until the shear stress at the end of the zone reaches the frictional stress. "Re-bonding" can occur, for example, when unloading takes place after the fibre at the adjacent end segment has reached the maximum load. It should be noted that the "re-bonded" zone is not really bonded, but that the shear flow is lower than the frictional bond. Therefore, another variable must be introduced, namely the "active debonded length" to distinguish between the bonded, unbonded, and "re-bonded" regions. The "re-bonded" zone returns to frictional as soon as the shear stress exceeds the frictional stress.

With the two-fibre system, the purely frictional bond theory cannot be used in a general case, even if the fibre has totally debonded. Theories in which a purely frictional bond is assumed have successively been used for the pull-out problem, or in single fracture analysis. One approach is to assume that the whole fibre force at the crack is transferred to the matrix along the length P/t_f [7] (Fig. 4a), but it was later noticed that the longitudinal displacement in the matrix may exceed that in the fibre, which is physically impossible [10]. The frictional bond theory can still be used if assuming a zero friction along the length where the strain in the fibre and the matrix are equal [15] (Fig. 4b).

Let us study a case, in the two-fibre system, in which the fibre and its symmetry fibre overlap within the fibre end segment (Fig. 4c). Before dynamic slip a point can be found where the strains in the fibre and the matrix are equal. If the shear flow continues as t_f, the strain in the matrix exceeds that in the fibre, which is physically impossible. On the other hand, if the shear flow becomes zero, the strain in the fibre exceeds that in the matrix and has to change again to t_f. An intermediate value $t_f/\hat{Q}$ for the shear flow would maintain equal strains in the fibre and the matrix. This contradicts the purely frictional theory with a single-valued shear flow. Therefore, it is suggested that along the region where the shear flow must be less than t_f, the full bond conditions prevail.

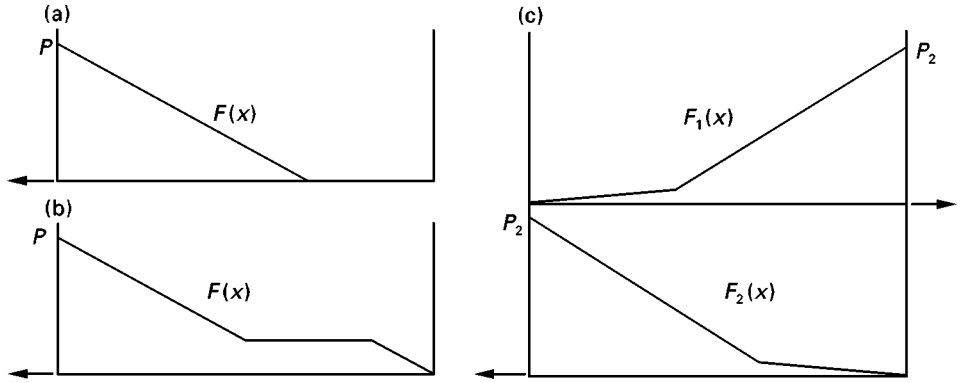

Figure 4 Theories of a frictional bond. (a) Shear flow, t_f, (b) shear flow, either t_f or zero, (c) shear flow t_f or $t_f/\hat{Q}$.

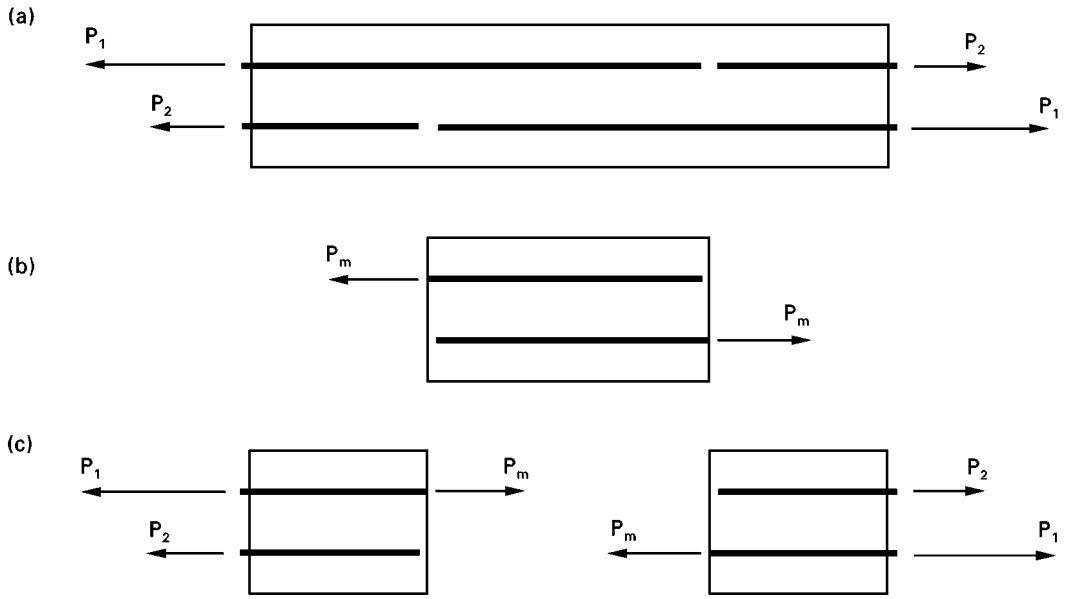

Figure 5 Two-fibre model at fibre end. (a) Whole segment, (b) overlapping region, and (c) non-overlapping regions.

The fibre breaks or yields if the stress exceeds the fibre tensile strength. When the fibre breaks, continuity at the crack disappears because even if the fibre forces at both sides of the cracks are equal, namely zero, the compatibility condition 18 is no longer valid. The coupling in the system equations at the breaking point disappears, and for computational efficiency, only that part of the fibre can be analysed where the results are needed for the statistical analysis of the composite. The breaking point now becomes the fibre end and must be analysed as such. In the case of fibre yielding, the condition is that the fibre force at the crack must be equal to the yield stress.

5. Fibre ends

In the statistical analysis the fibre volume content is assumed to be equal everywhere in the composite. Thus one fibre follows the other at the fibre end. The relative displacement of the fibre at the crack depends not only on the fibre force at the crack, but also on the fibre forces at the adjacent cracks. Hence there is coupling between subsequent fibres. In a general case, there would then be too many equations to solve; to limit their number only a single fibre is analysed at a time. This means that the coupling between subsequent fibres must be eliminated. Let P_1 be the first (or last) unknown fibre force in Equation 22 (see Fig. 5). To derive the fibre displacement at the crack, the fibre force P_2 in the subsequent fibre at the crack is needed. However, it is not included in the unknown variables, and must be approximated before analysis.

At the end segment, the fibre and its symmetry fibre may overlap, depending on the embedded length. If the fibres overlap, there are three regions, an overlapping and two non-overlapping lengths (Fig. 5). For all regions, separate equations must be formed. Between the regions a compatibility condition holds, which says that there is no crack, or that the relative displacements at both sides of the interface must be equal.

In the region where the fibres do not overlap, a single fibre system is assumed for the following reasons: first, the two-fibre system would be too complicated with respect to the attainable improvements, due to possible non-symmetry of debonded lengths (see Fig. 5c). Second, the fibre force at the adjacent crack has to be defined before analysis. If the fibre end

does not extend beyond the middle of the segment, it can be analysed independently without knowing the force in the other fibre. On the other hand, if the fibre ends overlap, the force in the other fibre is needed. The embedded length of this fibre is shorter than half the segment length, making it possible to obtain the predetermined force from an independent analysis. Third, in the limit case when the embedded length is either 0 or s, s being half the crack spacing, both methods lead to the same result. The validity of the simplified method must be studied for intermediate embedded lengths.

To study the validity of the simplified approach at the fibre ends, where the non-overlapping regions are treated as independent, some example calculations were performed for the fibre end segment using both theories. The bond was assumed to be elastic. The relative fibre displacements at both cracks were assumed to be equal to 0.01 μm. The geometrical and material parameters were as follows: crack spacing $2s = 10$ mm, shorter fibre embedded length $l = 3$ mm, moduli ratio of the matrix and the fibre $E_f/E_m = 100$, and fibre diameter $d = 0.5$ mm. The fibre volume content, V_f, and thus the bond modulus, κ, varied. A large ratio of elastic moduli was chosen, as this leads to the greatest inaccuracy compared with the two-fibre analysis.

The examples were analysed using fibre volume contents of $V_f = 5\%$, 10% and 30%, and bond moduli of $\kappa = 2.10 \times 10^{12}$, 2.68×10^{12}, and 5.58×10^{12} N m^{-3}, respectively. Relative errors of the forces in the fibre at the cracks, the force in the matrix in the middle of the segment, and the average matrix force due to the simplified approach were computed and are shown in Table I.

TABLE I Relative errors (%) of forces in the fibre at the cracks, the force in the matrix in the middle of the segment, and the average matrix force, due to the simplified approach at the fibre end

E_f/E_m	V_f (%)	Fibre force at left crack	Fibre force at right crack	Matrix force in the middle	Average matrix force
100	5	6.0	− 6.6	1.5	2.1
100	10	23.0	− 15.8	6.3	11.1
100	30	63.8	− 28.0	4.0	73.1
10	30	1.1	− 1.1	0.1	5.1

The simplified approach was found to give too high a fibre force for the shorter fibre, and too low a force for the longer fibre. It also resulted in higher shear stresses at the fibre ends, affecting the ability of debonding onset at the embedded end to be predicted at a smaller crack width. In addition, it gave a higher matrix force, leading to an exaggerated composite strain approximation, or to prediction of cracking at a too low a load level.

Another analysis was performed with a lower stiffness ratio of $E_f/E_m = 10$, $V_f = 30\%$, and $\kappa = 6.18 \times 10^{13}$ N m^{-3}. Fig. 6 shows the distributions of the fibre force, the interfacial shear stress, and the matrix force. The relative errors are shown in Table I. The relative errors were found to increase with

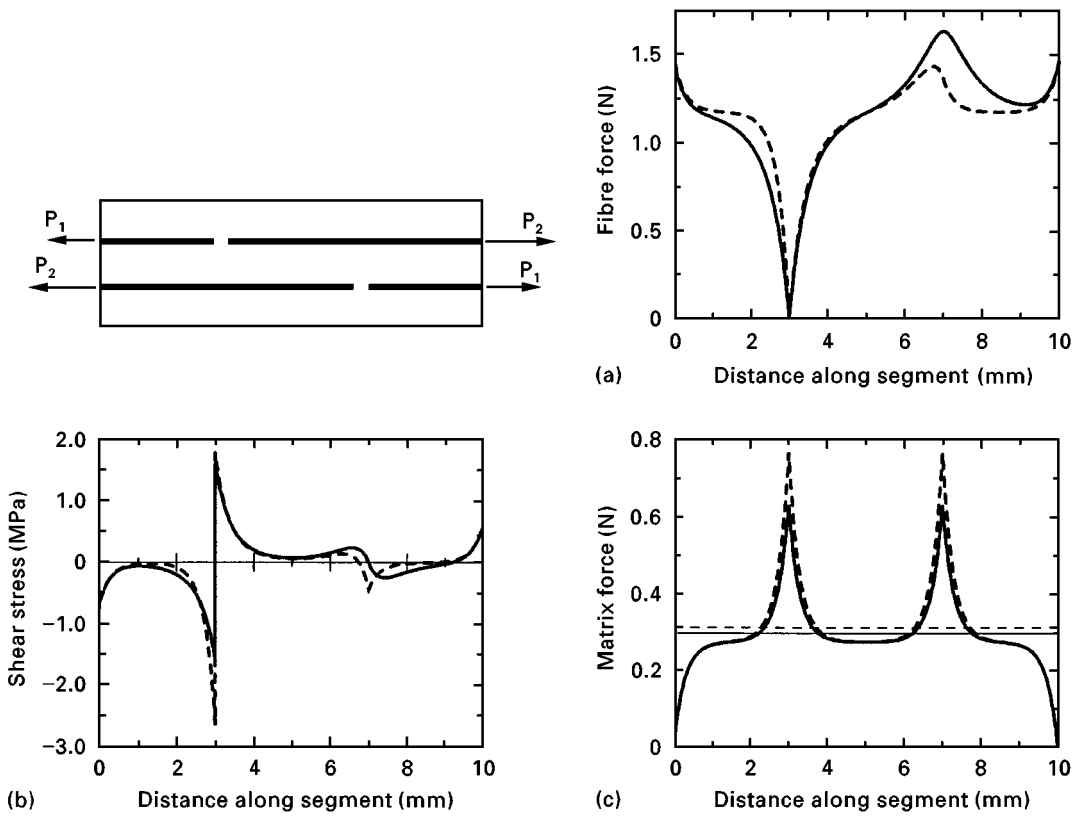

Figure 6 Distributions of (a) fibre force, (b) interfacial shear stress and (c) the matrix force for the fibre end segment, with $E_f/E_m = 10$, $V_f = 30\%$, and $\kappa = 6.18 \times 10^{13}$ N m^{-3}. The horizontal lines represent the average matrix force. (—) Two-fibre system, (– – –) independent fibres.

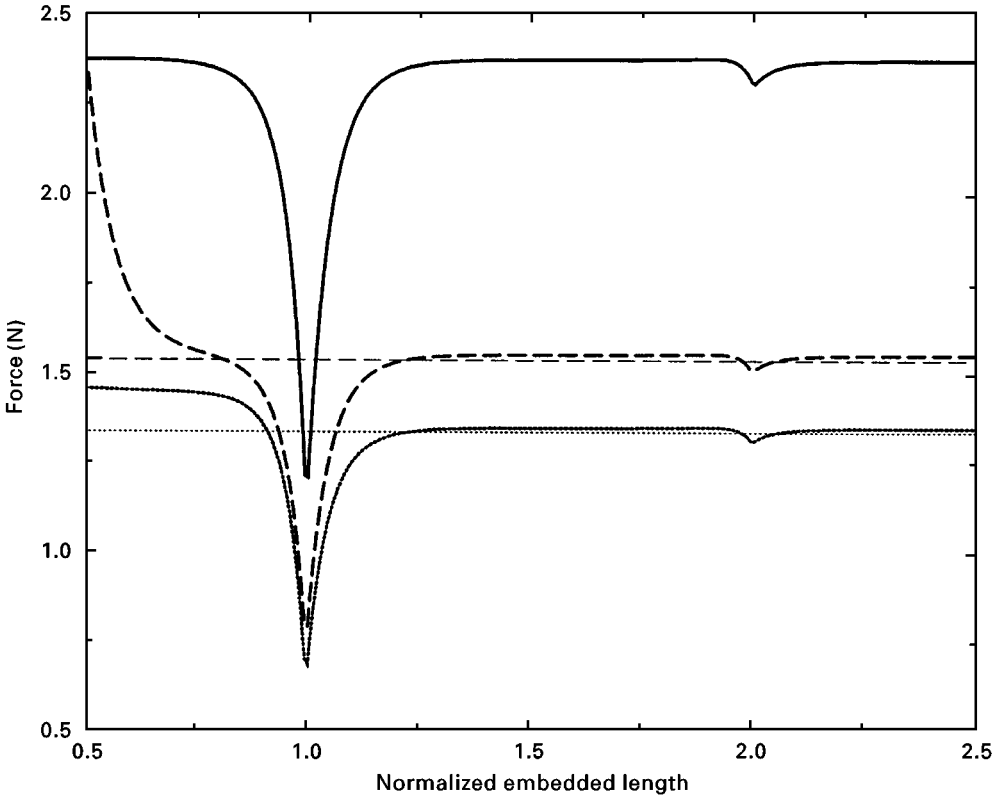

Figure 7 (—) Sum of adjacent fibre forces at the crack, (– – –) the matrix force in the middle of the segment, and (- - -) the average matrix force within the segment as a function of normalized fibre embedded length. The horizontal lines represent the mean values of the curves.

increasing fibre content, and to decrease with decreasing stiffness ratio E_f/E_m. If the stiffness ratio is less than 10, and if the fibre volume content is less than 30%, the errors of the simplified approach are less than 5.1%. For a stiffness ratio of 100, the accuracy of the simplified approach is reasonable only for low fibre contents.

In order to study whether the fibre end region has any effect on the matrix force compared with a continuous fibre, an analysis was performed in which the fibre location varied. In this way, a relationship between the matrix force and the fibre embedded length could be obtained. The following material parameters were chosen for the composite: moduli of elasticity of fibre and matrix $E_f = 210\,\text{GPa}$ and $E_m =$ GPa, respectively, fibre length $l_f = 50\,\text{mm}$, fibre diameter $d = 0.5\,\text{mm}$, fibre volume content $V_f = 5\%$, and bond modulus $\kappa = 2.48 \times 10^{13}\,\text{N m}^{-3}$. A crack spacing of $2s = 12.5\,\text{mm}$, and crack width $w = 0.048\,\mu\text{m}$ were chosen. It was also assumed that the fibre is oriented perpendicular to the cracks, and that full bond exists. Fig. 7 shows the sum of the fibre forces at adjacent cracks, the matrix force in the middle of the segment, and the average matrix force within the segment as a function of the normalized fibre embedded length $l/2s$.

In the end segment, the sum of the fibre forces decreases as the embedded end approaches the segment width. Correspondingly, the embedded length of the subsequent fibre at the adjacent crack approaches zero. Therefore, its contribution at a normalized embedded length of 1 is zero. The matrix force decreases with increasing embedded length. On the other hand, as the normalized embedded length approaches 1/2, the matrix force in the middle of the segment approaches that of the fibres at the crack. This is because at the normalized embedded length of 1/2, the fibre ends are located in the middle of the segment and have zero forces, hence the total force is only carried by the matrix.

It can be seen that when the fibre extends beyond the segment ($l/2s$), the forces are of equal magnitude, with the exception of an embedded length of twice the crack spacing, when the forces tend to be somewhat lower. Because in this case the fibre embedded lengths at the end segments are $2s$, the forces at the outmost cracks are decreased, affecting the forces at the other cracks.

The horizontal lines in Fig. 7 represent the mean values of the two curves for the matrix forces. As can be seen, the fibre end region has little effect on the mean value of the average matrix force or on the mean value of the matrix force in the middle of the segment. On the other hand, the mean fibre force at the crack is seen to decrease due to the fibre discontinuity. It should be noted that the mean value of the fibre force is computed using embedded lengths from 0 to $l_f/2$, while the mean values for the matrix forces are calculated using the region from s *to* $s + l_f/2$. Therefore the average fibre force is not shown in Fig. 7. Nevertheless, it can be estimated given that the curve corresponding to the sum of the fibre forces with normalized embedded lengths varying from 0 to 1/2 is the mirror image of the curve with normalized embedded lengths varying from 1/2 to 1.

6. Examples

In this section, the problem of a fibre bridging several cracks is studied by solving Equation 22 and plotting the fibre force and the interfacial shear stress distributions along the fibre at different crack widths. The effect of different micromechancial parameters on fibre mechanics are described in an internal report [27]. The parameters include the stiffness ratio of fibre and matrix, the fibre volume content, the fibre diameter, or aspect ratio, and the interfacial frictional shear stress. Because according to the ACK theory (Aveston, Cooper and Kelly [1]), the crack spacing can vary between certain values, its effect is studied below. Consider the following material parameters as an example.

Matrix:

+ modulus of elasticity $E_m = 21\,\text{GPa}$
+ tensile strength $\sigma_{mu} = 5\,\text{MPa}$.

Fibres:

+ modulus of elasticity $E_f = 210\,\text{GPa}$
+ diameter $d = 0.5\,\text{mm}$
+ length $l_f = 40\,\text{mm}$
+ volume content $V_f = 5\%$.

Interface:

+ bond modulus $\kappa = 2.48 \times 10^{13}\,\text{N m}^{-3}$
+ shear strength $\tau_u = 4\,\text{MPa}$
+ frictional shear stress $\tau_f = 3\,\text{MPa}$.

A crack spacing of $2s = 5\,\text{mm}$ is chosen according to the ACK model, which gives a maximum crack spacing of 4.45 mm for a composite with aligned short fibres and a purely frictional stress transfer.

The fibre being analysed is aligned with the direction of the external load. The location with respect to the cracks is such that the fibre and its symmetry fibre overlap at the left end, but not at the right end. Moreover, the tensile strength of the fibre is chosen to be so large that fibre rupture does not occur.

The force and the interfacial shear stress distributions at three different crack widths are shown in Fig. 8. It can be seen that at a crack width of less than 0.3 μm, the bond is elastic, and no iteration is needed for solution of Equation 22. At a crack width of $w = 1\,\mu\text{m}$, debonding has progressed in all segments, and the debonded zones can be seen as a constant shear stress in the figure. The fibre's right end is totally debonded, resulting in a lower force at the crack than at the other cracks. The absolute values of the shear stresses ahead of the debonded zones are equal to the shear strength. However, at the second segment from the right, the shear stress ahead of the frictional zone is equal to the frictional stress due to the "re-bonding" discussed in Section 4. The debonding progress to a certain distance until the peak stress is reached. Thereafter, the fibre unloads, causing the shear stress in the elastic region ahead of the frictional zone to decrease below the frictional value. The length of the frictional zone is then gradually decreased until the shear stress in the "re-bonded" zone reaches the frictional stress. Before the onset of strain-softening (bottom of Fig. 8), the fibre slips within several segments. The above comment on "re-bonding" holds also here.

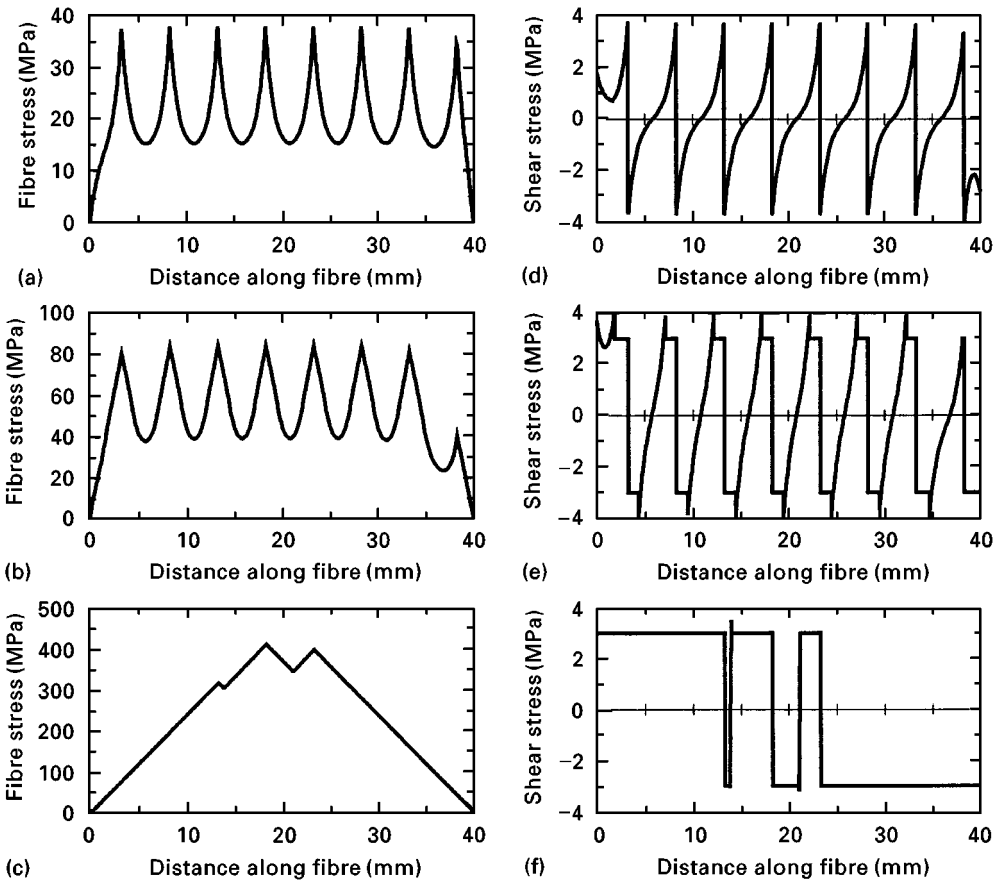

Figure 8 (a–c) Fibre force and (d–f) interfacial shear stress distributions along a fibre with crack spacing $2s = 5$ mm of (a, d) $w = 0.3\,\mu\text{m}$, (b, e) $w = 1.0\,\mu\text{m}$, (c, f) $w = 12.3\,\mu\text{m}$.

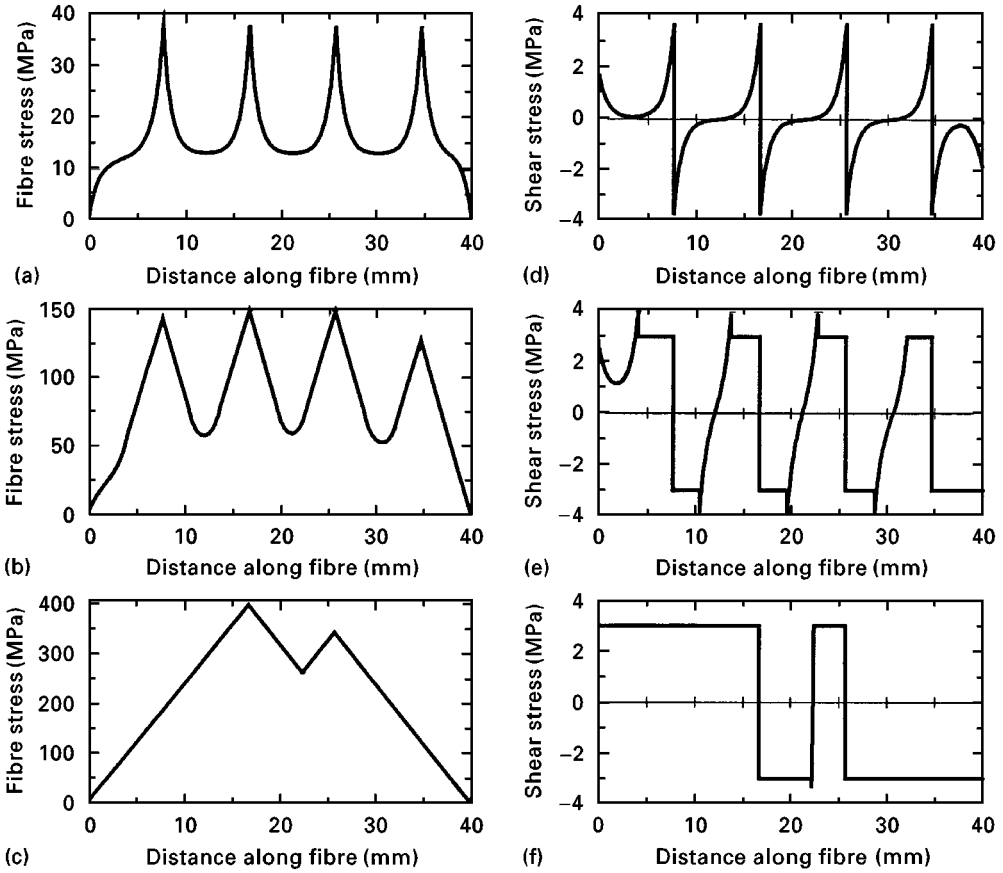

Figure 9 (a–c) Fibre force and (d–f) interfacial shear stress distributions along a fibre with crack spacing $2s = 9$ mm. (a, d) $w = 0.3$ μm, (b, e) $w = 3.0$ μm, (c, f) $w = 21.0$ μm.

The fibre is also analysed with the maximum crack spacing of $2s = 9$ mm, and the results are shown in Fig. 9. Now the fibre crosses only four cracks, and from the distribution of interfacial shear stress in the full bond stage, it can be seen that the curve becomes horizontal in the middle of the segment, indicating that the strains in the fibre and the matrix are equal without stress transfer between the constituents. Compared with the case of a 5 mm crack width (Fig. 8), it is seen that the fibre forces and the crack widths at the onset of debonding are equal for both crack spacings, but the force transferred to the matrix is higher with a larger crack spacing. At the peak stress, the fibre stresses are also equal, whereas the maximum crack width is large with higher crack spacing.

7. Conclusion

The micromechanical modelling of brittle-matrix composites reinforced with discontinuous fibres has been extended to the multiply-cracked stage. In this paper, the mechanics of a straight, smooth fibre bridging one or several cracks is studied. The analysis is based on the assumption of a symmetry fibre, which together with the fibre in question satisfies the equilibrium condition. The gradual debonding and pull-out are included, assuming that once the shear stress at the interface exceeds the shear strength, the bond fails and a constant frictional bond prevails. However, if the shear stress ahead of the debonded zone falls below the frictional stress, part of the frictional region "rebonds" and is analysed as having an elastic bond.

The force distributions within a segment are described as functions of the forces in the fibres at the cracks. The fibre displacements at the cracks relative to the matrix are calculated for different cases of debonded lengths. Using the compatibility condition of the crack width, the system equations can be stated and the unknown fibre forces and the rigid body displacements solved.

Because the fibre is not continuous, there is a discontinuity at the fibre end which has to be analysed separately. A simplified approach has been used, which assumes that fibre regions which do not overlap their symmetry fibre behave independently and are thus analysed using a single-fibre theory. Only the fibre ends overlapping are analysed as a two-fibre system. This assumption is accurate, if the fibre/matrix stiffness ratio or the fibre volume content are not too high.

The fibre discontinuity has an effect on the forces in the fibre and the matrix. However, in the elastic bond stage, it did not seem to affect the mean value of the average matrix force or the mean value of the matrix force in the middle of the segment. On the other hand, the mean fibre force at the crack was seen to be lower due to the fibre discontinuity. In the frictional stage, the difference between the continuous and the discontinuous fibre is remarkable. The forces in the continuous fibre are equal at adjacent cracks and the

load can be increased until the fibre breaks, whereas the discontinuous fibre would rather slide out and the maximum load at the crack depends on the embedded length.

The model of a fibre bridging several cracks will be used in a statistical model to compute the mechanics of a composite under a uniaxial tensile load. The composite model is described in Part II [28].

Acknowledgements

This study was carried out in the Netherlands, at Delft University of Technology, Faculty of Civil Engineering, and at TNO Building and Construction Research as part of a European Community research training project "Constitutive modelling of fibre-reinforced brittle materials for numerical analysis" under the programme "Training and Mobility of Researchers" financed by the European Commission.

Appendix. Analysis of fibres within a segment

When the fibre extends through the segment, different cases have to be analysed depending on how far the debonding has propagated. In every analysis the force distributions in the fibres and the relative displacements at the cracks are derived. The force distributions are given in Equations 5 and 6 for the full bond case, and in Equation 10 for fibre 1, if fibre 2 is debonded. A corresponding distribution is derived for fibre 2, if fibre 1 is debonded. Let l_1 and l_2 be the left and right debonded lengths, respectively, for fibre 1, and the right and left debonded lengths, resepctively, for fibre 2. l is the length of the whole segment and s half the segment length.

Four different cases can be deduced. The full bond case is reported elsewhere [22], and the other cases in an internal report [27]. Consider the case $l_1 < s, l_2 < s$ as an example. If debonding from neither of the cracks has progressed further than the middle segment, there exist regions with only a frictional bond at the ends, only an elastic bond in the middle and, between them, regions with both an elastic and a frictional bond (Fig. A1). Let l_1 be greater than l_2. Then the force distributions in the fibres are

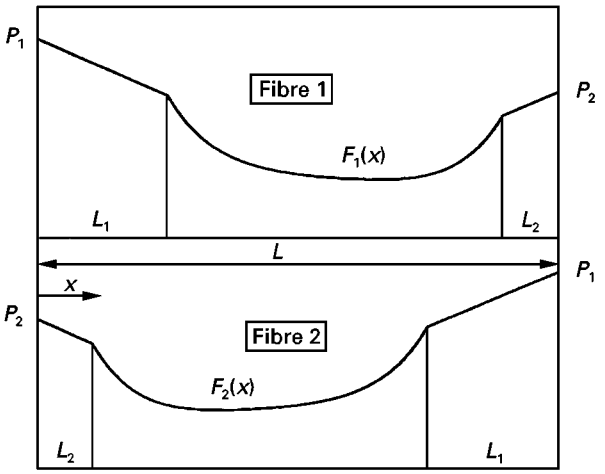

Figure A1 A1 Distributions of fibre forces where both ends are debonded less than in the mid-segment.

where t_f^l and t_f^r are the frictional shear flows between fibre 1 and the matrix on the left and right side of the segment, respectively. For fibre 2, t_f^l is the right, and t_f^r the left frictional shear flow. Their absolute values are equal, but their sign depends on the direction of friction. It should be noted that t_f^l is negative in Fig. A1. Moreover, $P_1 = F_1(0) = F_2(l)$, and $P_2 = F_1(l) = F_2(0)$.

The continuity and symmetry conditions

$$F_1(l_1) = P_1 + t_f^l l_1 \tag{A3a}$$

$$F_1(s) = F_2(s) \tag{A3b}$$

$$F_1'(s) = -F_2'(s) \tag{A3c}$$

$$F_1(l-l_1)^- = F_1(l-l_1)^+ \tag{A3d}$$

$$F_1'(l-l_1)^- = F_1'(l-l_1)^+ \tag{A3e}$$

$$F_1(l-l_2) = P_2 - t_f^r l_2 \tag{A3f}$$

from which the coefficients $A-F$ can be solved as functions of P_1 and P_2. The strain differences between

$$F_1(x) = \begin{cases} P_1 + t_f^l x & 0 \leqslant x < l_1 \\ Ae^{-\lambda_1 x} + Be^{\lambda_1 x} + Ce^{-\lambda_2 x} + De^{\lambda_2 x} + \dfrac{P}{\hat{Q}+1} & l_1 \leqslant x < l-l_1 \\ Ee^{\hat{\lambda}x} + Fe^{-\hat{\lambda}x} + \dfrac{1}{\hat{Q}}[P_2 + t_f^l(x-l)] & l-l_1 \leqslant x \leqslant l-l_2 \\ P_2 + t_f^r(x-l) & l-l_2 < x \leqslant l \end{cases} \tag{A1}$$

$$F_2(x) = \begin{cases} P_2 - t_f^r x & 0 \leqslant x < l_2 \\ Ge^{\hat{\lambda}x} + He^{-\hat{\lambda}x} + \dfrac{1}{\hat{Q}}(P_2 - t_f^l x) & l_2 \leqslant x < l_1 \\ -Ae^{-\lambda_1 x} - Be^{\lambda_1 x} + Ce^{-\lambda_2 x} + De^{\lambda_2 x} + \dfrac{P}{\hat{Q}+1} & l_1 \leqslant x \leqslant l-l_1 \\ P_1 - t_f^l(x-l) & l-l_1 < x \leqslant l \end{cases} \tag{A2}$$

the fibres and the matrix are [22]

$$\varepsilon_{f1} - \varepsilon_m = \frac{1}{2A_mE_m}(\hat{Q}F_1 - P + F_2) \qquad (A4)$$

$$\varepsilon_{f2} - \varepsilon_m = \frac{1}{2A_mE_m}(\hat{Q}F_2 - P + F_1) \qquad (A5)$$

The relative displacements at the cracks are calculated by:

$$\Delta_1 = \frac{1}{\psi\kappa}\frac{dF_1}{dx}\bigg|_{x=l_1} - \int_{l-l_1}^{l}(\varepsilon_{f2} - \varepsilon_m)\,dx$$

$$= \frac{1}{\psi\kappa}(-\lambda_1 Ae^{-\lambda_1 l_1} + \lambda_1 Be^{\lambda_1 l_1} - \lambda_2 Ce^{-\lambda_2 l_1} + \lambda_2 De^{\lambda_2 l_1})$$

$$- \frac{1}{2A_mE_m}\left\{(\hat{Q} - 1)\,P_1 l_1 - P_2(l_1 - l_2)\right.$$

$$+ \tfrac{1}{2}\hat{Q}t_f^1 l_1^2 - \tfrac{1}{2}t_f^r l_2^2 + \frac{E}{\hat{\lambda}}[e^{\hat{\lambda}(l-l_2)} - e^{\hat{\lambda}(l-l_1)}]$$

$$- \frac{F}{\hat{\lambda}}[e^{-\hat{\lambda}(l-l_2)} - e^{-\hat{\lambda}(l-l_1)}]$$

$$\left. + \frac{1}{\hat{Q}}[P_2(l_1 - l_2) - \tfrac{1}{2}t_f^1(l_1^2 - l_2^2)]\right\} \qquad (A5)$$

$$\Delta_2 = \frac{1}{\psi\kappa}\frac{dF_1}{dx}\bigg|_{x=l-l_2} + \int_{l-l_2}^{l}(\varepsilon_{f1} - \varepsilon_m)\,dx$$

$$= \frac{1}{\psi\kappa}\left[\hat{\lambda}Ee^{\hat{\lambda}(l-l_2)} - \hat{\lambda}Fe^{-\hat{\lambda}(l-l_2)} + \frac{t_f^1}{\hat{Q}}\right]$$

$$+ \frac{1}{2A_mE_m}\left[(\hat{Q} - 1)\,P_2 l_2 - \tfrac{1}{2}\hat{Q}t_f^r l_2^2 + \tfrac{1}{2}t_f^1 l_2^2\right] \qquad (A6)$$

where Δ_1 and Δ_2 are the displacements at the cracks where the fibre forces are P_1 and P_2, respectively. The displacements are linear functions of P_1 and P_2. The coefficients of P_1 and P_2 are then added to the terms c_{ij} in Equation 22, while the constants are added to the right hand side vector $\boldsymbol{R}$.

References

1. J. AVESTON G. A. COOPER and A. KELLY, in "Single and multiple fracture", Proceedings of a Conference, National Physical Laboratories (IPC Science and Technology, Guildford, 1971) pp. 15–24.
2. A. E. NAAMAN and S. P. SHAH, in "Proceedings of the 11th National Symposium on Fracture Mechanics", edited by C. W. Smith and S. W. Freiman (American Society for Testing and Materials; Philadelphia, PA, 1979) pp. 183–201.
3. P. TJIPTOBROTO and W. HANSEN, *ACI Mater. J.* **90**(1) (1993) 16.
4. M. MAALEJ and V. C. LI, *ACI Struct. J.* **92**(2) (1995) 167.
5. J. AVESTON, R. A. MERCER and J. M. SILLWOOD, in "Fibre reinforced cements-scientific foundations for specifications. Composites-standards, testing and design", Proceedings, National Physical laboratory (IPC Science and Technology, Guildford, 1974) pp. 93–103.
6. A. E. NAAMAN, and H. NAJM, *ACI Mater. J.* **88**(2) (1991) 135.
7. Y. WANG, S. BACKER and V. C. LI, *Composites* **20** (1989) 265.
8. A. E. NAAMAN, G. G. NAMUR, J. M. ALWAN and H. S. NAJM, *J. Struct. Eng.* **117** (1991) 2769.
9. C. K. Y. LEUNG, *J. Eng. Mech.* **118** (1992) 2298.
10. C. K. Y. LEUNG and V. C. LI, *J. Mater. Sci.* **26** (1991) 5996.
11. H. STANG, Z. LI and S. P. SHAH, *J. Eng. Mech.* **116** (1990) 2136.
12. B. BUDIANSKY, J. W. HUTCHINSON and A. G. EVANS, *J. Mech. Phys. Solids* **34**(2) (1986) 167.
13. T. Y. LIM, P. PARAMASIVAM and S. L. LEE, *ACI Mater. J.* **84** (1987) 286.
14. C. -H. HSUEH, *Mater. Sci. Eng.* **A123** (1990) 1.
15. V. C. LI, H. STANG and H. KRENCHEL, *Mater. Struct.* **26** (1993) 486.
16. V. C. LI, Y. WANG and S. BACKER, *J. Mech. Phys. Solids* **39** (1991) 607.
17. J. KULLAA, *Composites* **25** (1994) 935.
18. J. AVESTON and A. KELLY, *J. Mater. Sci.* **8** (1973) 352.
19. P. TJIPTOBROTO and W. HANSEN, *ACI Mater. J.* **90** (1993) 134.
20. V. C. LI and C. K. Y. LEUNG, *J. Eng. Mech.* **118** (1992), 2246.
21. S. -H. LI, S. P. SHAH, Z. LI and T. MURA, *Int. J. Solids Struct.* **30** (1993) 1429.
22. J. KULLAA, *J. Mater. Sci.* **31** (1996) 61.
23. C. K. Y. LEUNG and V. C. LI, *Composites* **21** (1990) 305.
24. G. NAMMUR Jr and A. E. NAAMAN, *ACI Mater. J.* **86** (1989) 45.
25. V. C. LI and Y.-W. CHAN, *J. Eng. Mech.* **120** (1994) 707.
26. J. KULLAA, *J. Struct. Eng.* **122** (1996) 783.
27. J. KULLAA, "Micromechanics of multiple cracking. Crack Bridging". TUD report 03.21.0.22.21, Delft University of Technology, Faculty of Civil Engineering, Delft, (1996) 52 pp.
28. J. KULLAA, *J. Mater. Sci.* **33** (1998) 0000.

Received 21 February 1997
and accepted 15 May 1998